AD-A064 043 AIR FORCE INST OF TECH WRIGHT-PATTERSON AFB OHIO SCH--ETC F/G 17/8
SIGNAL PROCESSING FOR SHEARING INTERFEROMETER MEASUREMENTS.(U)
DEC 78 P J MARTONE

UNCLASSIFIED AFIT/GEO/EE/78-2 NL

1 OF 1
AD
A064 043

END
DATE
FILMED
4 -79
DDC

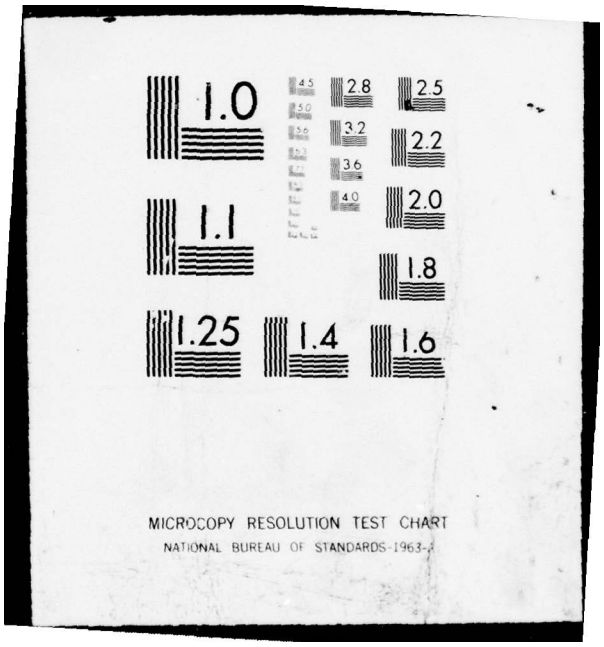
1.0
1.1
1.25
1.4
1.6
1.8
2.0
2.2
2.5
2.8
3.2
3.6
4.0
4.5
5.0
5.6
MICROCOPY RESOLUTION TEST CHART
NATIONAL BUREAU OF STANDARDS-1963-A

DDC

LEVEL

AIR FORCE INSTITUTE OF TECHNOLOGY

AIR UNIVERSITY
UNITED STATES AIR FORCE

SCHOOL OF ENGINEERING

WRIGHT-PATTERSON AIR FORCE BASE, OHIO

AFIT/GEO/EE/78-2

LEVEL II

AD A064043

DDC FILE COPY.

SIGNAL PROCESSING FOR SHEARING INTERFEROMETER MEASUREMENTS

THESIS

AFIT/GEO/EE/78-2 Patrick J. Martone
2nd Lt USAF

Approved for public release; distribution unlimited

AFIT/GEO/EE/78-2

(14)

(6) SIGNAL PROCESSING FOR SHEARING INTERFEROMETER MEASUREMENTS.

(9) Master's THESIS,

Presented to the Faculty of the School of Engineering

of the Air Force Institute of Technology

Air Training Command

in Partial Fulfillment of the

Requirements for the Degree of

Master of Science

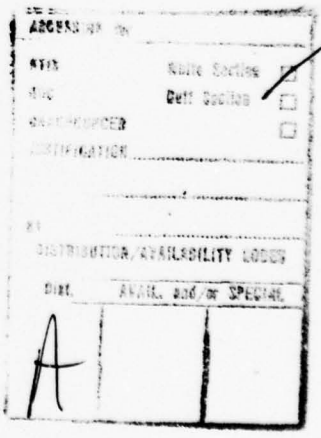

by

(10) Patrick J. Martone

2nd Lt USAF

Graduate Electro-Optics

(11) Dec [redacted] 78 (12) 61 p.

Approved for public release; distribution unlimited

012 225

PREFACE

This thesis assumes the reader has a working knowledge of random processes, Fourier and Laplace transforms, and linear systems theory.

I am deeply grateful for the assistance of my advisor, Captain Stanley R. Robinson. His guidance and optimistic tone proved to be essential for the production of this paper.

I would like to thank Lt Paul Idell for his many stimulating discussions and suggestions. My other friends, Lt Billy Newton, Lt Robert Mason, and Lt John Santiago, also deserve thanks for their exchange of ideas which kept us all going through this period.

Finally, I would like to thank Cindy Held for the excellent typing of this thesis.

Patrick J. Martone

Contents

List of Figures

Notation

a_j	Expansion coefficients
a_0	Bandwidth of power spectral density for θ
$\underline{a}$	(6×1) vector containing (a_1- a_6)
B_1	Bandwidth of the basic demodulation scheme
B_2	Bandwidth of the phaselocked loop configuration
d	Grating period defined by $2\pi r/N$
dB	Decibel
D	Real amplitude
e(t)	Error signal
E[ ]	Expectation value
E(x,y)	Optical field defined by $E_0 \exp[jk\cos\theta x]$
E_0	Real amplitude of E(x,y)
f	Focal length
f_x	Spatial frequency defined by $x/\lambda f$
f_y	Spatial frequency defined by $y/\lambda f$
f(t)	Time response of the filter F(s)
F(s)	Filter for phaselocked loop
F[ ]	Fourier transform
g( )	Grating amplitude transmittence function
$H_\phi(s)$	Closed loop transfer function of the phaselocked loop configuration

I_d	Intensity at the detector plane
k	Propagation constant defined by $2\pi/\lambda$
K_1	Amplitude of the VCO output
$K_2(t)$	Kalman gain
K_{VCO}	Gain of the VCO
K	Defined by $K_1 K_{VCO} M$
M	The multiplier gain
$n_1(t), n_2(t)$	Statistically independent zero mean random noise terms
$n'(t), n''(t)$	Defined by $n'(t) = n_1(t)\cos\theta(t) + n_2(t)\sin\theta(t)$, $n''(t) = -n_1(t)\sin\theta(t) + n_2(t)\cos\theta(t)$
$n_i(t)$	Narrowband random process defined by $n_1(t) = n_c \cos w_0 t - n_s \sin w_0 t = N_i(t)\cos(w_0 t + \theta_i(t))$
$N_i(t)$	Envelope of the noise
N	Number of pairs of radial spokes
$N_0/2$	Amplitude of the autccorrelation of the noise
$P(t)$	The variance of Φ
q	Defined by $r\int_0^t w_1(\alpha)d\alpha - \cos\theta$
r	Radius of rotating Ronchi grating
$r(t)$	Estimate signal generated by the phaselocked loop
$R_\theta(0)$	Autocorrelation of θ at $\tau = 0$

$R_{N_c}(\tau)$	Autocorrelation of N_c
s	Shear distance defined by $\lambda f/d$
$S_{N_c}(s)$	Power spectral density of N_c
$S_\theta(s)$	Power spectral density of θ
$S_w(s)$	Power spectral density of w
s(t)	Detector signal
SNR	Signal to noise ratio
t_d	Delay time
U(,)	Electric field
v	Linear velocity
V_0, V_{+1}, V_{-1}	Three electric fields at the detector plane
w_0	Rotation rate of the Ronchi grating
w(,)	Incoming field
z	Optic axis
z_0, z_1, z_2	Locations along the optic axis
$Z_1(\rho)$ - $Z_6(\rho)$	Orthonormal polynomials related to Zernike polynomials
δ( )	Dirac delta function
η	Defined by $\lvert\rho\rvert$
θ	Phase of a detector signal
λ	Optical wave legnth

ξ	Receiving aperture function
σ^2	Variance
ϕ	Phase of the optical field
ψ	Defined by $\frac{2\pi f}{d}\cos\theta$

ABSTRACT

This paper provides a basic description of the operation of a shearing interferometer used for phasefront sensing. The signal processing of the interferometer's outputs are studied. A basic demodulation scheme and a phaselocked loop configuration are discussed and compared. Some elementary phaselocked loop theory is prcvided. A possible configuration using optical feedback for determining off-axis tilt of a plane is presented. The signal-to-noise ratio of the shearing interferometer's outputs is improved by a slight modification of the optical configuration. Finally, a geometric representation of a distorted phase profile is provided which will describe the deleterious effects of a planar phasefront propagating through the turbulent atmosphere.

I Introduction

The turbulent atmosphere, which is sometimes referred to as a random inhomogeneous medium, distorts and deforms optical radiation as it propagates outward from its source (Refs. 1-3). That is, if a source is radiating quasi-monochromatic light (Ref. 4, pg 13), a distorted plane wave will be received in the far field. If this source were a laser, then its far field target would not receive a focused, intense beam because of atmospheric turbulence. The problem of maximizing the intensity of a laser beam on a far field target is evident.

It has been shown through reciprocity (Ref. 5) that an optical system which projects a laser beam onto a far field target will experience identical atmospheric turbulence effects as the image of a radiating target on the optical system. Therefore, if one can measure the phase profile of a target's radiation, then the effects of the turbulent atmosphere will be known. Compensation for these effects can then be made so that a laser beam will not suffer the same deleterious effects but will instead have maximum intensity on the target.

A common configuration for the optical system which compensates for atmospheric turbulence is shown in Figure 1. The telescope acts as the exit aperature for the laser beam and the receiving aperature of the target radiation. The optical radiation from the target enters the telescope, reflects off the tilt mirror, reflects off the deformable mirror, and upon incidence to the beamsplitter is reflected into the phasefront sensor. The phasefront sensor reconstructs the phase profile

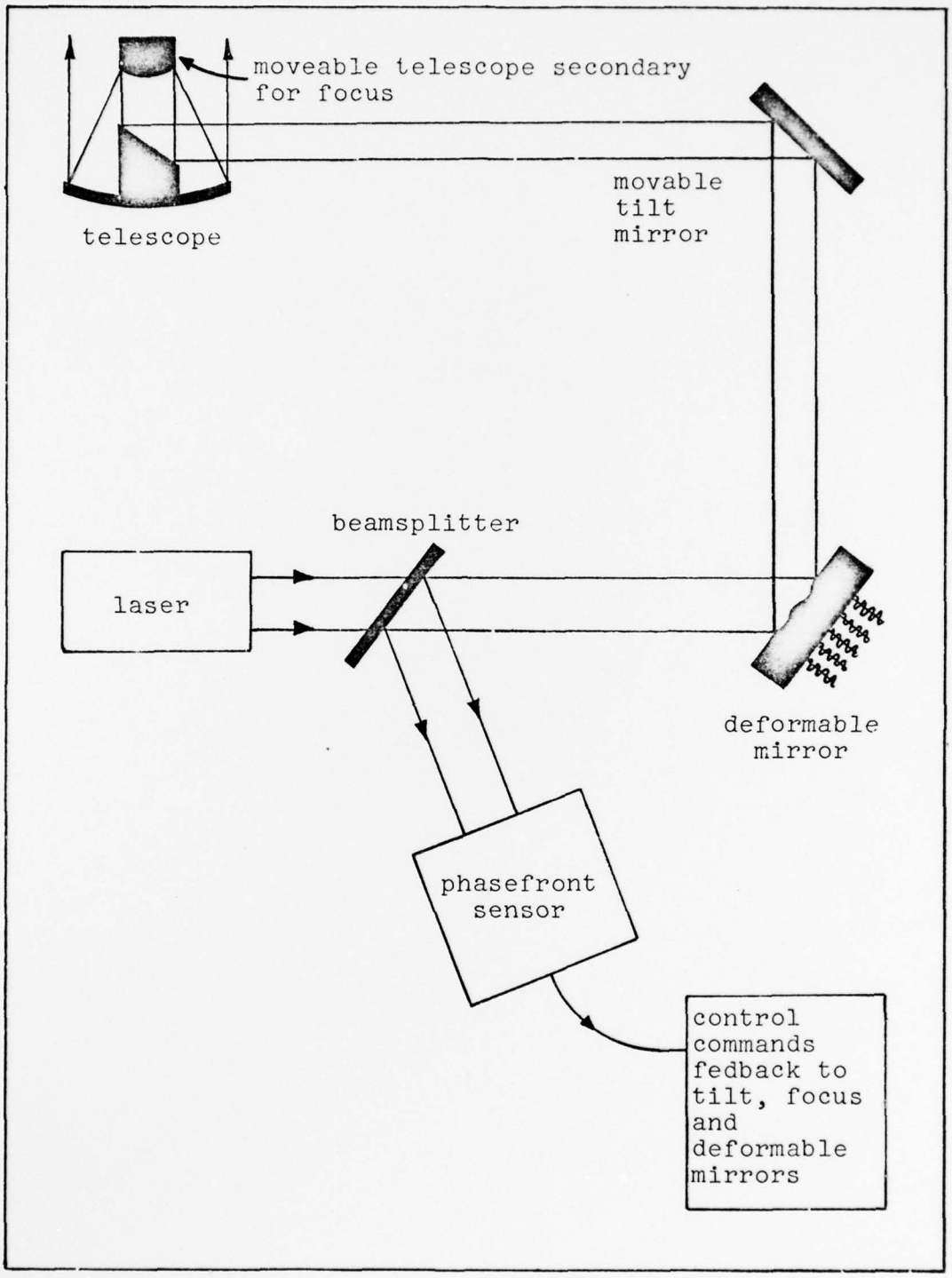

Figure 1. Basic configuration of complete optical system

of the target's radiation. Through appropriate signal processing of the reconstruction, the atmospheric turbulence can be compensated for so that the intensity of the laser beam is maximized on the target. This compensation is accomplished by control signals to the tilt, focus, and deformable mirrors.

The laser beam propagates through the beamsplitter, reflects off the deformable mirror, reflects off the tilt mirror, and exits the telescope to propagate through the turbulent atmosphere to the target.

The device of concern in this paper is the phasefront sensor. Specifically, a type of phasefront sensor referred to as a shearing interferometer is studied. Also the signal processing of the interferometer output is analyzed.

The following chapter provides a description of the shearing interferometer. Chapter 3 discusses the processing of detector signals using Phaselocked loop and Optimal Linear Filter theory. A geometric representation of a distorted phase profile is discussed in Chapter 4.

II Phasefront Measuring by use of a Shearing Interferometer

There are no direct detectors that can measure the phase of a field. Detectors measure the intensity of a field and thus phase information is lost. The shearing interferometer provides a solution to this problem.

A shearing interferometer (Refs. 6-9) is a phasefront sensor whose outputs can be used to reconstruct the phase profile or contour of the input optical field.

The basic components of a shearing interferometer are two Fourier transform lenses, a rotating Ronchi grating (Ref. 10, pg 207), and a detector array as shown in Figure 2.

In Figure 2 z_0, z_1, and z_2 are specific locations along the z or optic axis, and f is the focal length of lenses L_1 and L_2. The Ronchi grating consists of a circular disk with alternating clear and opaque radial lines extending from near the center to the outer edge (Ref. 9) as shown in Figure 3, pg 6.

The rotating Ronchi grating which has radius r, rotating at w_0 radians per second, and having N pairs of radial spokes will have a linear velocity of

$$v = w_0 r \tag{1}$$

and a grating period of

$$d = 2\pi r/N \tag{2}$$

At any radius the amplitude transmittance function of the grating can be approximated by a square wave, which can be

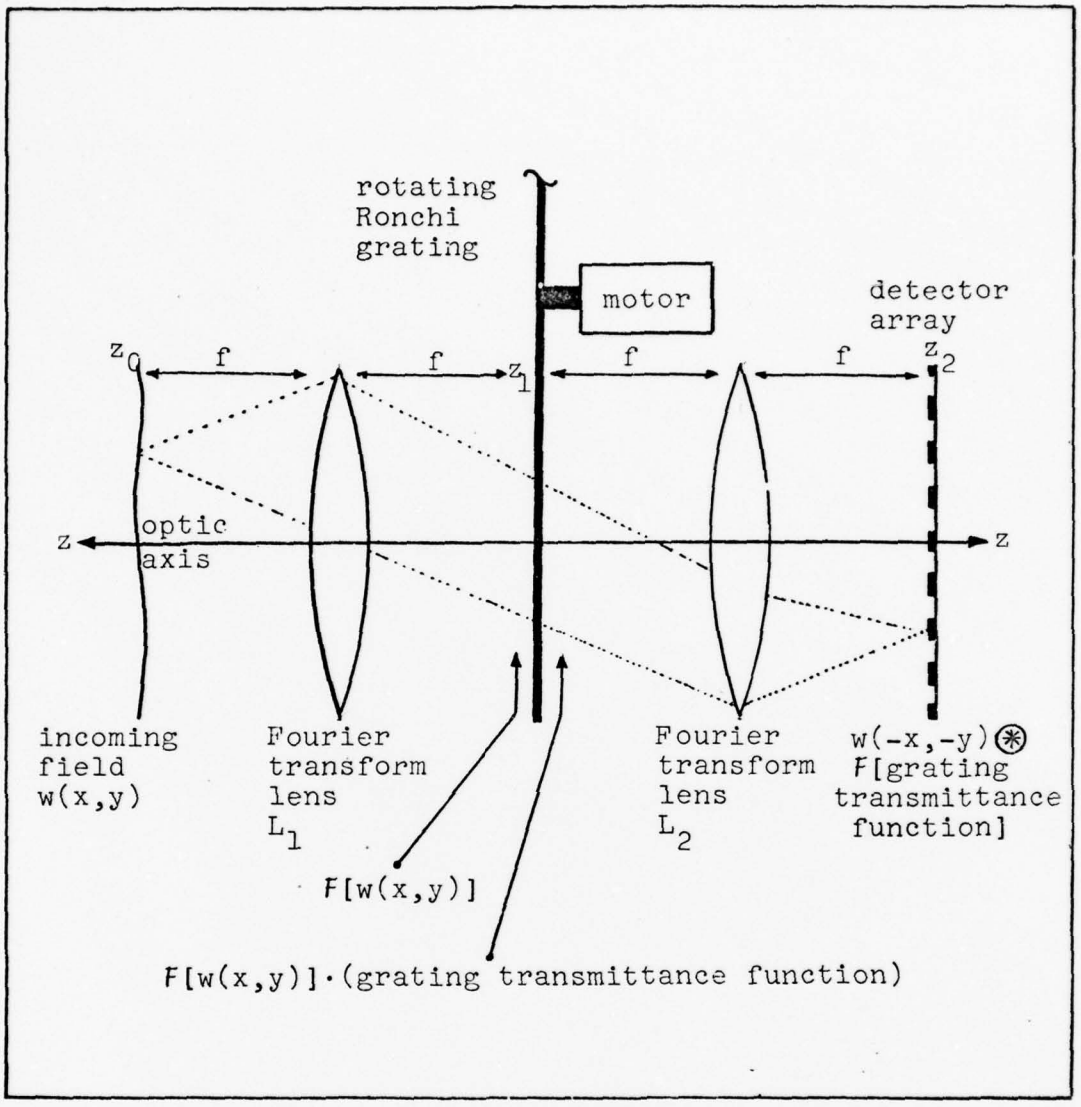

Figure 2. Shearing Interferometer

represented as the following Fourier series

$$g(x_1-vt) = \sum_n A_n \exp\,[+j2\pi n(x_1-vt)/d] \qquad (3)$$

where the A_n's are Fourier coefficients. The coefficients for the Ronchi grating are shown in Table 1. (Ref. 11, pg 28)

In the following analysis constant phase delay terms have

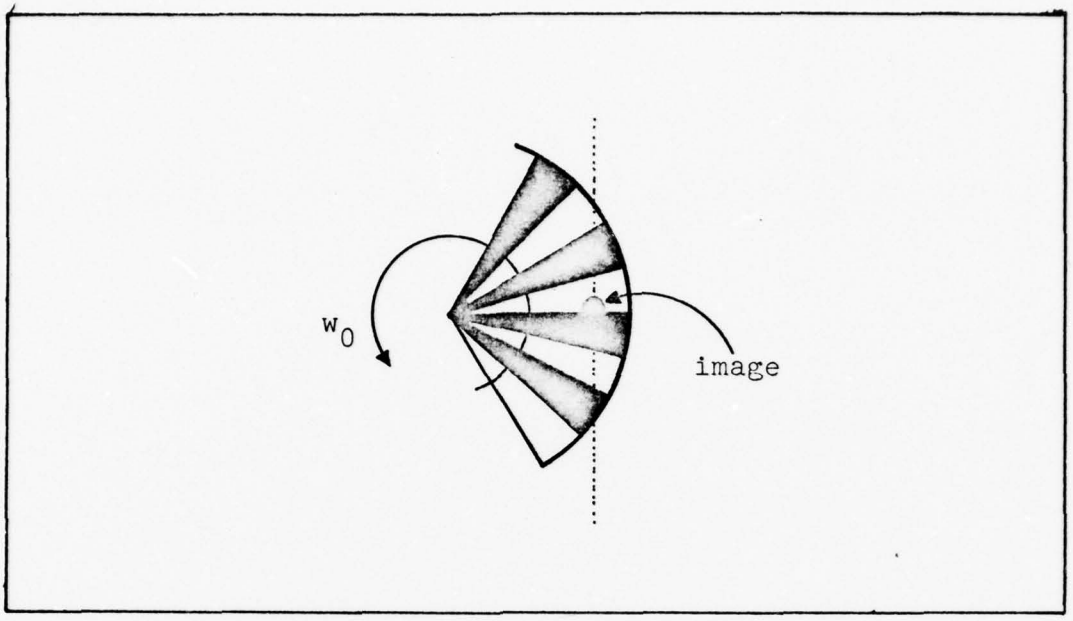

Figure 3. Rotating Ronchi grating

been neglected. A time dependence of $\exp[j2\pi f_0 t]$ for the incident quasimonochromatic field is assumed. When an incoming field $w(x_0,y_0) = A_{inc}(x_0,y_0)\exp[+j\phi(x_0,y_0)]$ (where A_{inc} is a real amplitude and x_0,y_0 are coordinates at z_0 of the optic axis) is located at f in front of lens L_1, the Fourier

order n	amplitude of A_n	phase of A_n	intensity
0	.5000	0°	.2500
±1	$1/\pi$	±90°	.1013
±2	0	-	-
±3	$1/3\pi$	±90°	.0112

Table 1. Fourier Coefficients for a Ronchi grating

transform of the wavefront

$$F[w(x_0,y_0)]\Big|_{\substack{f_x = x_1/\lambda f \\ f_y = y_1/\lambda f}} \propto W(x_1,y_1) \qquad (4)$$

is proportional to the field at the plane of the rotating grating. (x_1 and y_1 are coordinates at z_1 of the optic axis, f_x and f_y are spatial frequencies , and λ is the optical wavelength) Immediately following the grating the field becomes

$$U(x_1,y_1) \propto W(x_1,y_1)\cdot\sum_n A_n \exp[j2\pi n(x_1-vt)/d] \qquad (5)$$

At the detector plane (at location z_2 of the optic axis) the field becomes

$$F[U(x_1,y_1)]\Big|_{\substack{f_x = x_2/\lambda f \\ f_y = y_2/\lambda f}} \propto w(-x_2,-y_2) \circledast F[g(x_1-vt)]\Big|_{\substack{f_x = x_2/\lambda f \\ f_y = y_2/\lambda f}} \qquad (6)$$

where the symbol $\circledast$ represents a two dimensional convolution (Ref. 11, pg 82). The Fourier transform of equation (3) becomes

$$F[g(x_1-vt)]\Big|_{\substack{f_x = x_2/\lambda f \\ f_y = y_2/\lambda f}} \propto G(x_2-vt)$$

$$= \sum_n \exp[-j(k/f)x_2 vt]A_n \cdot \delta(x_2-n\lambda f/d)\delta(f_y) \qquad (7)$$

The above equation is nonzero only when $x_2 = n\lambda f/d$, and by substituting for x_2 in the first term of equation (7) we have $\exp[-j(k/f)x_2 vt] = \exp[-j2\pi nvt/d]$ where $w_0 = 2\pi nv/d$ is the modulated frequency of the electric field. Now equation (6) becomes

$$U(x_2,y_2) = F[U(x_1,y_1)]\Big|_{\substack{f_x = x_2/\lambda f \\ f_y = y_2/\lambda f}} \propto w(-x_2,-y_2)$$

$$\circledast \sum_{n=0,+1,-1} \exp[-jw_0 t] \cdot A_n\delta(x_2-n\lambda f/d) \cdot \delta(f_y) \qquad (8)$$

where n is restricted to 0, +1, and -1 since higher orders result in higher frequencies which are filtered out by the electronics. The above expression for the field at the detector plane shows that the shear distance is

$$s = \lambda f/d \qquad (9)$$

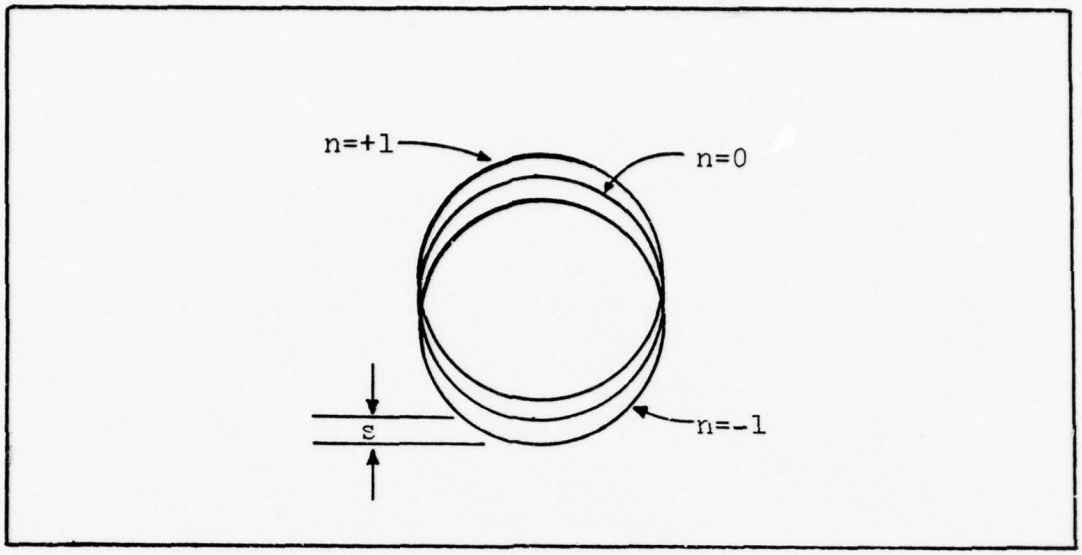

Figure 4. Shearing pattern produced at the detector plane

where λ is the wavelength of the field. Figure 4 shows the shearing pattern of the first three terms produced at the detector plane. The three electric fields of Figure 4 are

$$V_0 = A_0 A_{inc}(x_2,y_2)\exp[j\phi(x_2,y_2)]$$

$$V_{+1} = A_{+1} A_{inc}(x_2+s,y_2)\exp[j\phi(x_2+s,y_2)]\exp[-jw_0 t]$$

and

$$V_{-1} = A_{-1} A_{inc}(x_2-s,y_2)\exp[j\phi(x_2-s,y_2)]\exp[+jw_0 t] \quad (10)$$

where A_0, A_{+1}, and A_{-1} are found in Table 1. The total electric field at the detector plane is

$$U_d(x_2,y_2) = V_0 + V_{+1} + V_{-1} + \{\text{higher order terms}\} \quad (11)$$

where the higher order terms are neglected as they will be filtered out by the electronics. Since the detectors of the shearing interferometer measure intensity, the intensity of $U_d(x_2,y_2)$ becomes

$$I_d(x_2,y_2) = U_d(x_2,y_2)U_d^*(x_2,y_2)$$

$$= [V_0 + V_{+1} + V_{-1}][V_0 + V_{+1} + V_{-1}]^*$$

$$= V_0V_0^* + V_{+1}V_{+1}^* + V_{-1}V_{-1}^* + V_{+1}V_0^* + V_{+1}V_{-1}^*$$

$$+ V_{-1}V_0^* + V_{-1}V_{+1}^* + V_0V_{+1}^* + V_0V_{-1}^* \qquad (12)$$

where * denotes the complex conjugate of the designated quantity. For simplicity let $A_{inc}(x_2,y_2) = A_{inc}(x_2+s,y_2) = A_{inc}(x_2-s,y_2) = A_t$, then equation (12) becomes

$$I_d(x_2,y_2) = A_t^2 + \frac{2A_t^2}{\pi^2} + \{\text{time varying terms of frequency } 2w_0$$

$$+ \frac{A_t^2}{\pi}\cos(w_0t - 90° + \phi(x_2,y_2) - \phi(x_2+s,y_2))$$

$$+ \frac{A_t^2}{\pi}\cos(w_0t - 90° + \phi(x_2-s,y_2) - \phi(x_2,y_2)) \qquad (13)$$

(See Appendix for result when the sheared amplitudes are not equal.) The DC term $A_t^2 + 2A_t^2/\pi^2$, and the double frequency terms $2w_0t$ are also filtered out by the electronics, thus equation (13) reduces to

$$I_d(x_2,y_2) = \frac{2A_t^2}{\pi}\cos(w_0t - 90° + \frac{\phi(x_2-s,y_2) - \phi(x_2+s,y_2)}{2})$$

$$\cdot \cos(\frac{\phi(x_2-s,y_2) + \phi(x_2+s,y_2)}{2} - \phi(x_2,y_2)) \qquad (14)$$

Assuming the phase variation across a shear distance is small (that is $(\phi(x_2-s,y_2) + \phi(x_2+s,y_2))/2 \approx \phi(x_2,y_2)$) equation (14) becomes

$$I_d(x_2,y_2) \simeq \frac{2A_t^2}{\pi}\sin(w_0 t + \frac{\phi(x_2-s,y_2) - \phi(x_2+s,y_2)}{2}) \quad (15)$$

This result shows that the overlapping fields at the detector plane produces a signal whose phase is proportional to the phase difference or slope of the wavefront. Therefore, the shearing interferometer measures a set of phasefront profiles in the direction of the shear.

A phasefront sensor uses two shearing interferometers that produce shear in orthogonal directions (x and y) providing a two-dimensional representation of a distorted phasefront. For simplicity assume that there are twelve detectors (six for the x-channel interferometer and six for the y-channel interferometer) so that the phasefront sensor outputs twelve signals whose phases are phase differences that define the slope of the phasefront in two dimensions (Ref. 6, pg 668). In Figure 5 the detector arrangements are shown along with a phase map illustrating how the phase difference at each detector is derived. Detectors are located behind each subaperture labeled ϕ_1-ϕ_k for the x and y shear.

In order to obtain the actual phasefront a reconstruction process is necessary which uses the twelve phase difference measurements as shown by Hardy (Ref. 6, pg 669). The reconstructed phasefront can be represented by a set of orthonormal polynomials which will be described in Chapter 4. These polynomials will describe the amount of random tilt (x and y), defocus, and astigmatism that the received phasefront has suffered through its propagation through the turbulent atmosphere.

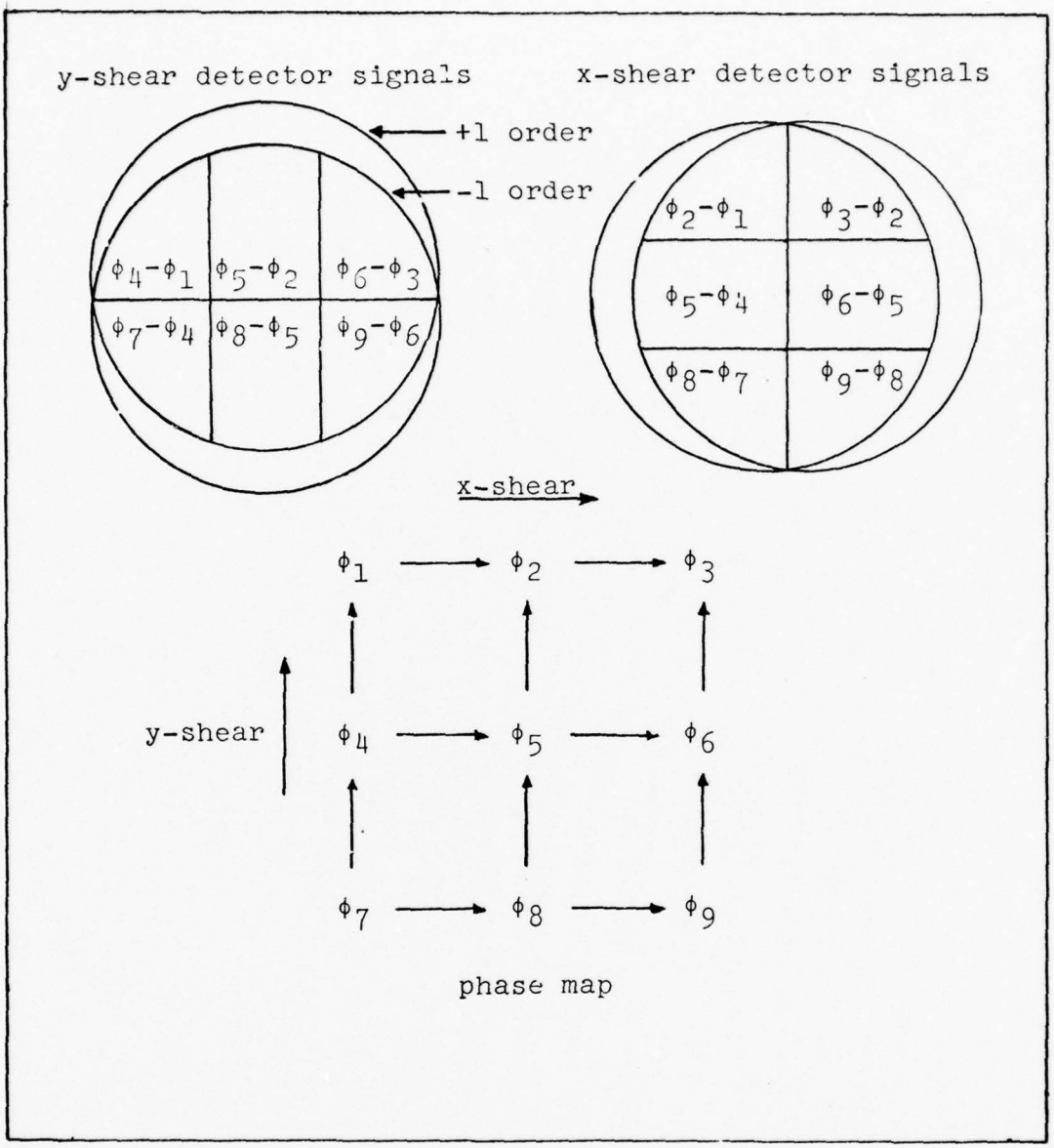

Figure 5. Phase difference measurements and location of detectors

Since it is the phase that is of interest, equation (15) for each of the twelve detectors must be demodulated in such a way that the phase term

$$\frac{\phi(x_2-s,y_2) - \phi(x_2+s,y_2)}{2} \tag{16}$$

is determined.

The actual intensity at the detector plane is very small compared to that at the input of the shearing interferometer due to the less than unity transmittance of the optics.

It can be shown that employing a sinusoidal grating instead of the Ronchi grating can increase the intensity at the detector plane. By using appropriate Fourier coefficients and equation (3), a result for any grating can be obtained.

The next chapter discusses possible configurations for determining the phase of a detector signal.

III Processing of Detector Signals

Basic Demodulation Scheme

A commonly proposed system for determing the phase of a signal is shown in block diagram form in Figure 6. The detector signal $s(t) = D\sin(w_0 t + \theta(t))$ (where D is a real amplitude and $\theta(t) = [\phi(t,x_2-s,y_2) - \phi(t,x_2+s,y_2)]/2$) enters a bandpass filter of center frequency $w_0/2\pi$. Then the signal is synchronously demodulated into two quadrature

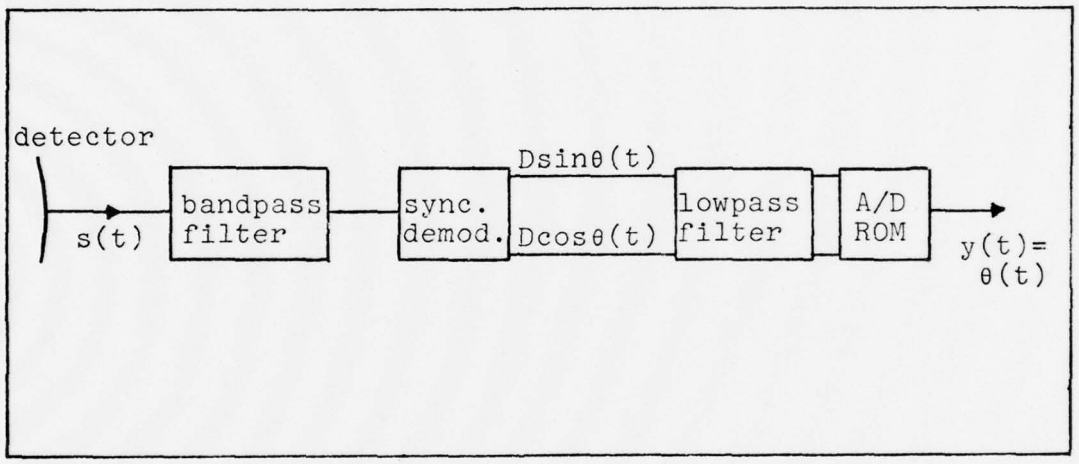

Figure 6. Basic demodulation scheme for detector signals

components $D\sin\theta(t)$ and $D\cos\theta(t)$, and lowpass filtered to eliminate some of the noise. The A/D ROM (analog-to-digital read-only-memory) performs an inverse tangent operation through a "table look-up" to determine θ.

For simplicity of analysis this scheme is studied on a continuum in time. Assuming the presence of bandpass, zero mean noise, the actual detector output becomes

$$s(t) = D\sin(w_0 t + \theta(t)) + n_1(t)\sin w_0 t + n_2(t)\cos w_0 t \tag{17}$$

where $n_1(t)$ and $n_2(t)$ are statistically independent zero mean random processes. The output of the scheme of Figure 6 would be (Ref. 12, pg 174-178)

$$y(t) = \theta(t) + \tan^{-1}\left(\frac{n''(t)}{D + n'(t)}\right) \tag{18}$$

where

$$n'(t) = n_1(t)\cos\theta(t) + n_2(t)\sin\theta(t)$$

$$n''(t) = -n_1(t)\sin\theta(t) + n_2(t)\cos\theta(t) \tag{19}$$

and $n'(t)$ and $n''(t)$ are zero mean random processes with distributions equal to those of $n_1(t)$ and $n_2(t)$. For the high signal to noise case (that is, Prob{n'>D} = Prob{n">D} ≈ 0) then equation (18) can be approximated by

$$y(t) \approx \theta(t) + \frac{n''(t)}{D} \tag{20}$$

The variance of equation (20) is derived as follows

$$E[y(t)] = \theta(t) \tag{21}$$

$$E[y^2(t)] = E\left[\theta^2(t) + 2\theta(t) \cdot \left(\frac{-n_1(t)\sin\theta(t) + n_2(t)\cos\theta(t)}{D}\right) + \left(\frac{-n_1(t)\sin\theta(t) + n_2(t)\cos\theta(t)}{D}\right)^2\right]$$

$$= \theta^2(t) + \frac{1}{D^2}E[n_1^2(t)]$$

$$= \theta^2(t) + \sigma_n^2/D^2 \tag{22}$$

where

$$\sigma_n^2 = E[n^2] = R_n(0)$$

$$= \int_{-B_1/2}^{-B_1/2} S_n(f)df = \frac{N_0 B_1}{2} \tag{23}$$

and B_1 is the bandwidth determined by the lowpass filter of Figure 6. Therefore, the variance of y(t) becomes

$$\sigma_y^2 = \frac{N_0 B_1}{2D^2} \tag{24}$$

This variance is an indication of how much on the average the random process y(t) fluctuates about its mean $\theta(t)$. The bandwidth B_1 must be selected large as compared to the bandwidth of a scheme which uses *a priori* knowledge of the process concerned. The phaselocked loop (PLL) is a scheme that uses some *a priori* information and is discussed in the next section. Some basic PLL theory will be provided first (Refs. 13, pg 66-84; 14, pg 127-131).

Basic Phaselocked Loop Theory

The Phaselocked loop configuration is used for measuring the phase of a signal. The basic elements of a PLL are a phase detector, a filter, and a voltage controlled oscillator (VCO) as shown in Figure 7. (The phase detector is represented as a multiplier.)

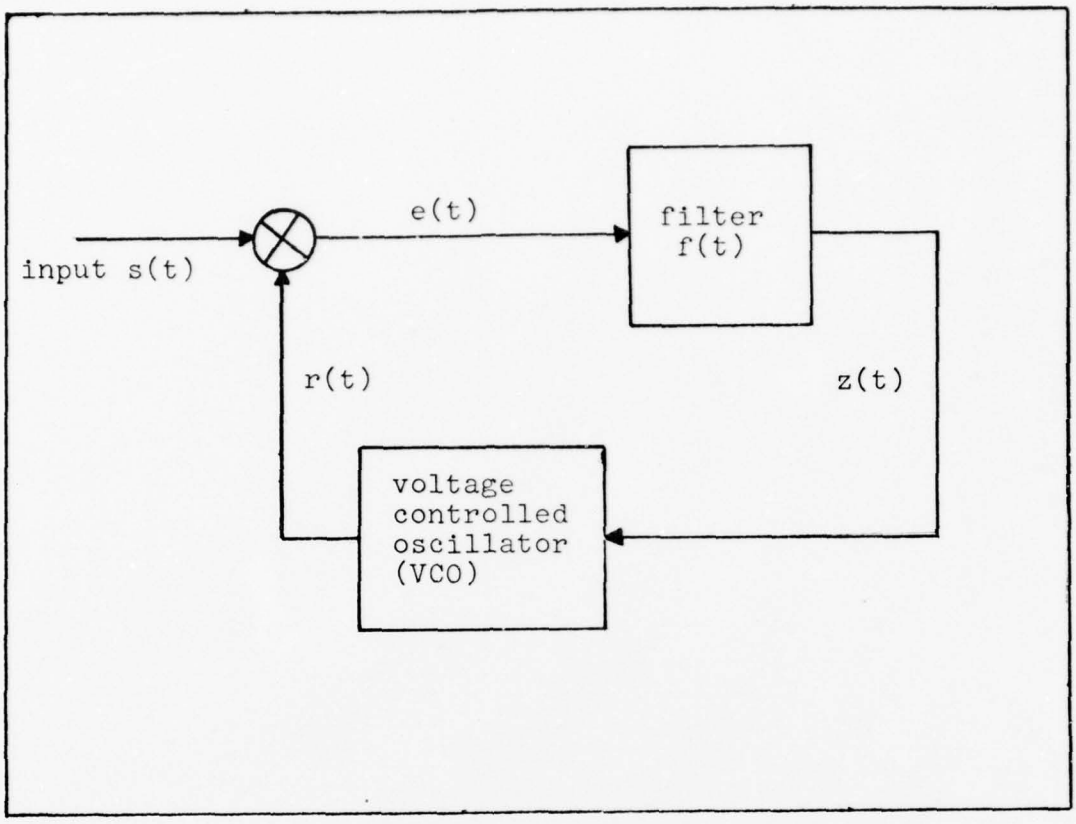

Figure 7. Simple Phaselocked Loop

The effective operation is dependent on the amount of *a priori* information that can be designed into the circuit. The PLL provides an estimate, r(t) of the input signal s(t), and by comparison, the loop continously modifies the local reference (VCO output) to reflect changes in the input. An error signal e(t) is produced at the output of the phase detector (the multiplier of Figure 7) if the input signal leads or lags the local reference. The error signal is filtered and sent back to the VCO in such a way as to change the frequency of the VCO so that it approaches the frequency of the input signal.

In order to determine the loop equation of the system, s(t) is considered to be a narrowband random process

$$s(t) = D\sin(w_0 t + \theta(t)) \tag{25}$$

and

$$r(t) = K_1 \cos(w_0 t + \hat{\theta}(t)) \tag{26}$$

where $\hat{\theta}(t)$ is the loop estimate of the input signal phase $\theta(t)$ in the absence of noise, and K_1 is the amplitude of the VCO output. The output of the multiplier e(t) neglecting double frequency terms becomes

$$e = DK_1 M \sin(\theta - \hat{\theta}) \tag{27}$$

where M is the multiplier gain. The argument $(\theta - \hat{\theta})$ is called the total loop phase error. The output of the filter with time response f(t) becomes

$$z(t) = e(t)F(s) \tag{28}$$

where F(s) is the Laplace transform of f(t) and the notation used is consistent with that of Lindsey (Ref. 13). (That is, equation (28) is equivalent to $z(t) = e(t) \circledast f(t)$.) The output phase of the VCO $\hat{\theta}$ referenced to zero is regarded to be a linear function of the control signal z(t). When z(t) is zero (which implies that e(t) is also zero) then the VCO outputs a constant quiescent frequency of w_0 radians/second. As mentioned earlier w_0 is also the frequency of the signal output from a detector. When z(t) is nonzero, then the VCO output becomes $w_0 + K_{VCO} z(t)$ where K_{VCO} is the gain of the voltage controlled oscillator (VCO) in units of radians per second per volt. The phase

estimate $\hat{\theta}$ developed by the loop is

$$\hat{\theta} = \frac{K_{VCO}z}{s} \tag{29}$$

where again the notation used is consistent with that of Lindsey. (The 1/s term is Laplace notation for the operation of integration.) Substituting for equation (27) and (28) into (29) yields

$$\hat{\theta} = \frac{DK_1K_{VCO}MF(s)}{s}\sin(\theta-\hat{\theta})$$

$$= \frac{DKF(s)}{s}\sin\Phi \tag{30}$$

where $K = K_1K_{VCO}M$ is the open loop gain and $\Phi = (\theta-\hat{\theta})$. Since $\hat{\theta} = \theta-\Phi$, equation (30) becomes

$$\Phi = \theta - \frac{DKF(s)}{s}\sin\Phi \tag{31}$$

Equation (31) is the equation for the PLL in the absence of noise.

In the presence of noise, the input of Figure 7 becomes $x(t) = s(t) + n_i(t)$. Now the error signal $e(t)$ depends not only on the total loop error $\Phi(t)$ but also the noise. The noise $n_i(t)$ is assumed to be a narrowband random process

$$n_i(t) = n_c\cos w_0t - n_s\sin w_0t \tag{32}$$

$$= N_i(t)\cos(w_0t + \theta_i(t)) \tag{33}$$

where $N_i(t)$ is the envelope of the noise and $\theta_i(t)$ is the random

phase. From equation (33) we have

$$n_c = N_i\cos\theta_i$$

and

$$n_s = N_i\cos\theta_i \tag{34}$$

The input now becomes

$$x(t) = D\sin(w_0t + \theta(t)) + N_i(t)\cos(w_0t + \theta_i(t))$$

$$= (D-N_s)\sin(w_0t + \theta(t)) + N_c\cos(w_0t + \theta(t)) \tag{35}$$

where $N_c = N_i\cos(\theta_i-\theta)$ and $N_s = N_i\sin(\theta_i-\theta)$. The error signal then becomes

$$e = K_1M[(D-N_s)\sin(\theta-\hat{\theta}) + N_c\cos(\theta-\hat{\theta})] \tag{36}$$

Once again the double frequency terms have been neglected. Since $\hat{\theta}(t) = K_{VCO}z(t)/s$, and $z(t) = F(s)e(t)$, then

$$\hat{\theta} = \frac{KF(s)}{s}[D\sin(\theta-\hat{\theta}) + N(t)] \tag{37}$$

where

$$N(t) = N_c\cos(\theta-\hat{\theta}) - N_s\sin(\theta-\hat{\theta}) \tag{38}$$

From equation (38) it is obvious that the noise is a function of the phase error $(\theta-\hat{\theta})$. Rearranging equation (37) the following is a nonlinear integrodifferential equation of the system

$$(\theta-\hat{\theta}) \triangleq \Phi = \theta - \frac{KF(s)}{s}[D\sin(\theta-\hat{\theta}) + N(t)] \tag{39}$$

The baseband loop model which equation (39) represents is shown in Figure 8.

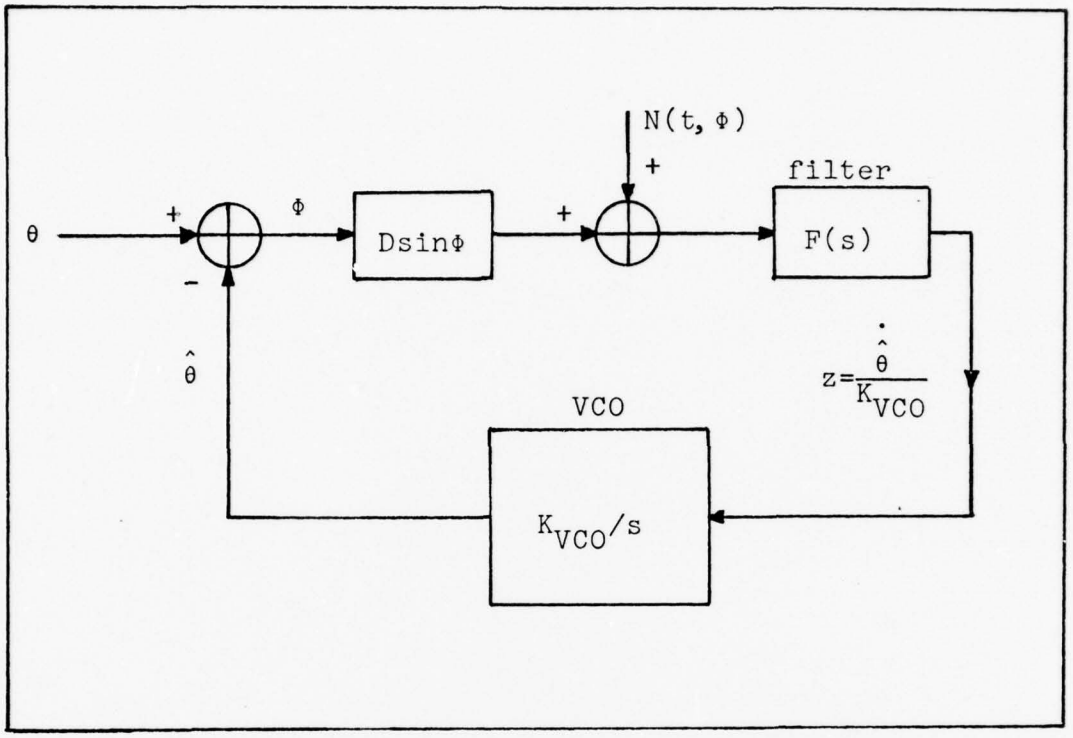

Figure 8. Baseband PLL model in the presence of noise

If the phaselocked loop is capable of reducing the phase error to a small value, then the approximation $\sin\Phi \approx \Phi$ becomes valid. Equation (39) then becomes

$$\Phi \triangleq (\theta-\hat{\theta}) = \theta - \frac{KF(s)}{s}\,[D\Phi + N_c\cos\Phi - N_s\sin\Phi]$$

$$\approx \theta - \frac{KF(s)}{s}\,[D\Phi + N_c] \qquad (40)$$

since $\sin\Phi \approx \Phi$ implies that $\cos\Phi \approx 1$, and $N_c >> N_c\Phi$. The linear baseband model which represents equation (40) is shown in Figure 9.

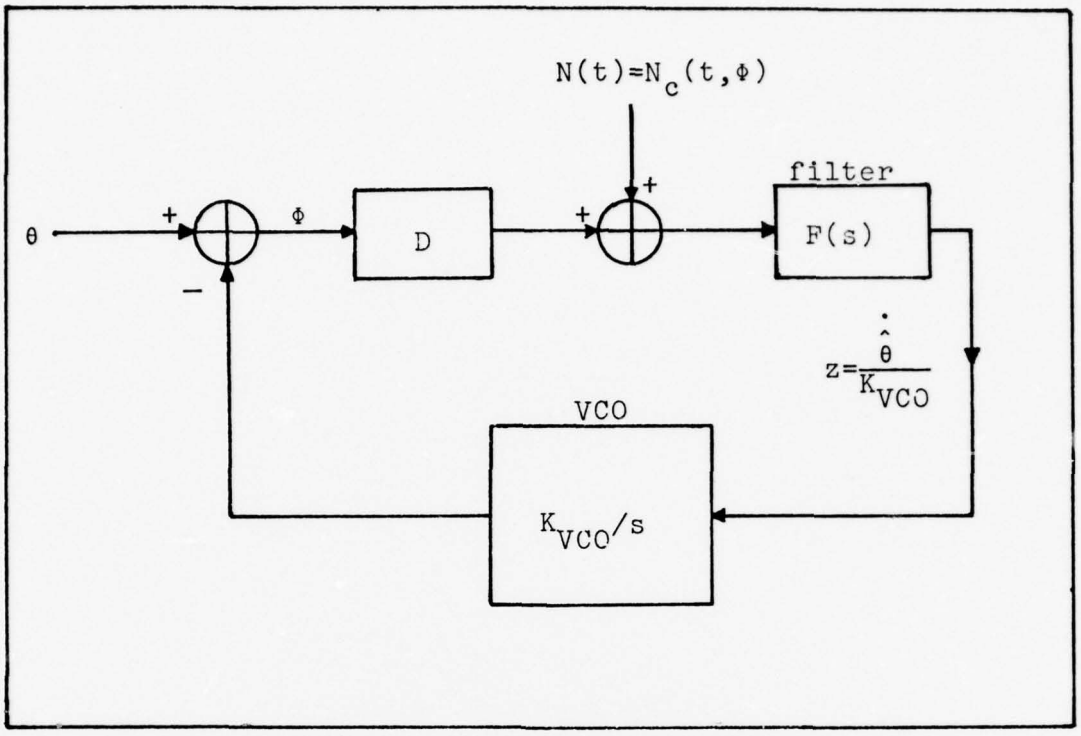

Figure 9. Linear baseband PLL model in the presence of noise

It can be shown (Ref. 13, pg 81-82) that

$$R_{N_c}(\tau) \simeq \frac{N_o}{2}\,\delta(\tau) \tag{41}$$

Therefore, the noise process $\{ N_c(t,\Phi) \}$ is white. Solving equation (40) for Φ yields

$$\Phi = \left(\frac{s}{s + DKF(s)}\right)\theta - \left(\frac{DKF(s)}{s + DKF(s)}\right)\frac{N_c}{D} \tag{42}$$

The closed loop transfer function of Figure 9 is

$$H_\Phi(s) \triangleq \frac{\hat{\theta}(s)}{\theta(s)} = \frac{DKF(s)}{s + DKF(s)} \tag{43}$$

Therefore equation (42) becomes

$$\Phi = \text{closed loop phase error}$$

$$= [1 - H_\Phi]\theta - [H_\Phi]\frac{N_c}{D} \tag{44}$$

where phase error can be caused by both the process θ changing faster than the loop can track and by the noise N_c. Equation (44) shows that there will be no contribution to the phase error by θ as long as $[1 - H_\Phi]$ is sufficiently highpass so that its spectrum doesn't overlap with that of θ. For this case the phase error will be dependent solely on the noise. The variance of the phase error in this case is

$$\sigma_\Phi^2 = \int_{-B_2/2}^{+B_2/2} |H_\Phi(s)|^2 \frac{S_{N_c}(s)}{D^2}\, ds$$

$$= \frac{B_2 N_0}{2D^2} = 1/SNR \tag{45}$$

where B_2 is the loop bandwidth, and $N_0/2$ is the power spectral density of N_c. As seen in equation (45) the phase error (due to noise only) is inversely proportional to the signal to noise ratio. The loop bandwidth B_2 should be considerably less than B_1 of equation (24) since some *a priori* statistics have been designed into the PLL circuit.

The phaselocked loop has been shown to exhibit the property of threshold extension, that is smaller signals can result in

similar performance (Ref. 15, pg 359). This extension is typically on the order of 2 or 3dB (Ref. 14, pg 291).

In the next section the filter F(s) of Figure 9 is designed so that the resulting variance of the phase error is minimized. The section will include the contributions of both θ and noise to the phase error.

Optimal Filter Design for the PLL Scheme

In this section the filter F(s) of Figure 9 is designed so that the resulting variance of the phase error is minimized. If Φ of equation (44) is a random process then (letting $E[\theta]=0$)

$$E[\Phi] = 0 \tag{46}$$

since N_c is a zero mean white process with autocorrelation

$$R_{N_c}(\tau) = E[N_c(t)N_c(t+\tau)] = \frac{N_0}{2}\delta(\tau) \tag{47}$$

From equation (44) we have

$$E[\Phi^2] = \sigma_\Phi^2 = \int_{-\infty}^{+\infty} |1 - H_\Phi(s)|^2 S_\theta(s)ds + \int_{-\infty}^{+\infty} |H_\Phi(s)|^2 S_{n'}(s)ds \tag{48}$$

where

$$S_{n'}(s) = \frac{N_0}{2D^2} = \frac{S_{N_c}(s)}{D^2} \tag{49}$$

Equation (48) is to be minimized by the following procedure.

The random process θ is assumed to be zero mean with a first order Butterworth power spectral density (Ref. 16, pg 502)

$$S_\theta(s) = \frac{2Q/a_0}{1 + (s/a_0)^2} \tag{50}$$

where $R_\theta(\tau) = F[S_\theta(s)] = Q\exp[-a_0\tau]$, a_0 is the bandwidth and the variance of θ is

$$\sigma_\theta^2 = R_\theta(0) = Q \tag{51}$$

With the above statistics, a simple filter model for the random process θ is derived. Let $w(t)$ be white gaussian noise with

$$E[w(t)] = 0 \ , \tag{52}$$

$$E[w(t)w(t+\tau)] = R_w(\tau) = 2a_0Q\delta(\tau) \tag{53}$$

and

$$S_w(s) = 2a_0Q \tag{54}$$

There exists a filter $H(s)$ such that the following is true

$$S_\theta(s) = |H(s)|^2 S_w(s) \tag{55}$$

and

$$H(s)H^*(s) = S_\theta(s)/S_w(s) \tag{56}$$

where * denotes the complex conjugate of the designated quantity. Substituting into equation (56) gives

$$H(s)H^*(s) = \frac{1/a_0^2}{1 + (s/a_0)^2} \tag{57}$$

Therefore

$$H(s) = \frac{1}{s + a_0} \tag{58}$$

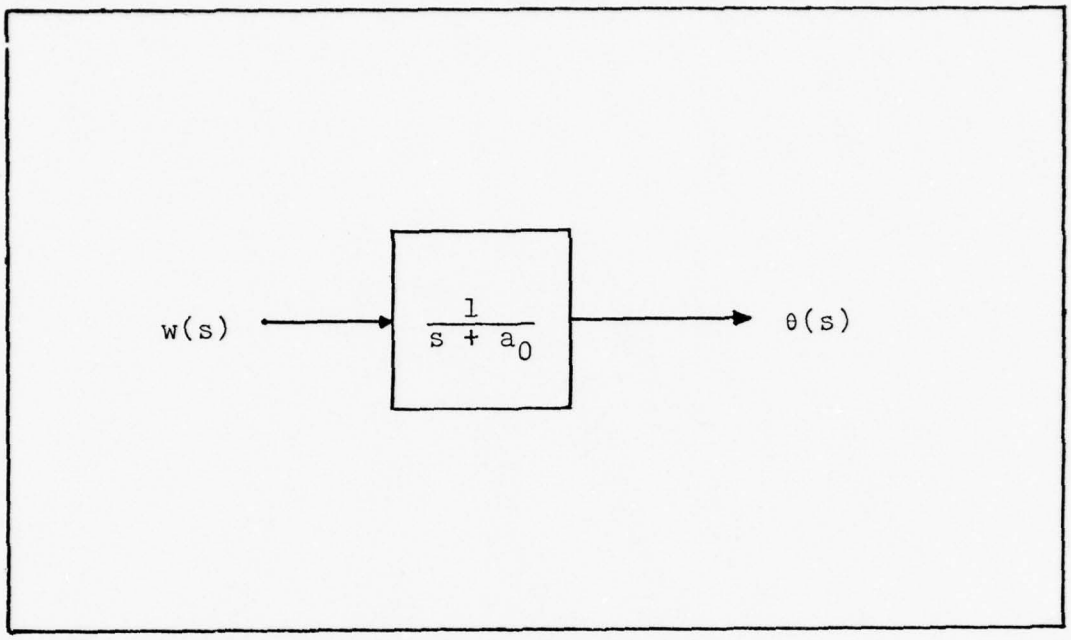

Figure 10. Model of the random process θ

The process θ is therefore modeled as shown in Figure 10. From Figure 10 we have

$$\frac{\theta(s)}{w(s)} = \frac{1}{s + a_0} \tag{59}$$

and

$$\dot{\theta}(s) = -a_0\theta(s) + w(s) \tag{60}$$

which is the first order state variable equation defining the random process θ.

In order to find the minimum value of σ_Φ^2, continuous Kalman filter equations are used to design an optimal filter F(s) in Figure 9. (See Ref. 17, pg 103-124 for the development of the continuous Kalman filter equations.) From Figure 9 we have

$$y(t) = D\theta(t) - D\hat{\theta}(t) + N_c(t,\Phi) \tag{61}$$

Using Table 4.3-1, pg 123, Ref. 17, the state estimate becomes

$$\begin{aligned}\dot{\hat{\theta}} &= -a_0\hat{\theta}(t) + K_2(t)[y(t) - (D\hat{\theta}(t) - D\hat{\theta}(t))] \\ &= -a_0\hat{\theta}(t) + K_2(t)y(t)\end{aligned} \tag{62}$$

where $K_2(t) = 2P(t)D/N_0$ is the Kalman gain and $P(t)$ is the variance of Φ . The Ricatti equation for $P(t)$ becomes

$$\dot{P}(t) = -2a_0P(t) + 2a_0Q - \frac{2P^2(t)D^2}{N_0} \tag{63}$$

For steady state set $\dot{P}(t) = 0$ and the minimum value of the variance becomes

$$\sigma_\Phi^2 = P_{\substack{\text{steady}\\\text{state}}} = \frac{-N_0a_0}{2D^2} + \frac{1}{2D^2}\sqrt{N_0a_0(N_0a_0 + 4D^2Q)} \tag{64}$$

where the plus sign of the quadratic equation has been chosen since the variance must be positive. The steady state Kalman gain becomes

$$\begin{aligned}K_{2_{\substack{\text{steady}\\\text{state}}}} &= \frac{2P_{\substack{\text{steady}\\\text{state}}}D}{N_0} \\ &= \frac{-a_0 + \frac{1}{N_0}\sqrt{N_0a_0(N_0a_0 + 4D^2Q)}}{D}\end{aligned} \tag{65}$$

Equation (62) then becomes

$$\dot{\hat{\theta}} = -a_0\hat{\theta} + y\,\frac{-a_0 + \frac{1}{N_0}\sqrt{N_0a_0(N_0a_0 + 4D^2Q)}}{D} \qquad (66)$$

and rearranging yields

$$\hat{\theta} = y\left[\frac{-a_0 + \frac{1}{N_0}\sqrt{N_0a_0(N_0a_0 + 4D^2Q)}}{D}/(s + a_0)\right] \qquad (67)$$

From Figure 9 it is obvious that the output of the filter F(s) must be $\dot{\hat{\theta}}/K_{VCO}$ when the input is y. Therefore F(s) becomes

$$F(s) = \frac{s\left[\frac{-a_0 + \frac{1}{N_0}\sqrt{N_0a_0(N_0a_0 + 4D^2Q)}}{D}\right]}{K_{VCO}(s + a_0)} \qquad (68)$$

which is the steady state optimal filter that results in a minimum value of the variance of the error stated by equation (64). (Note that the derived equations (64) and (68) agree with equations (4-105) and (4-104) of Ref. 13, pg 63 for the case where n=1, Q=1, k=1, K_t=1, and $C(k)=4R=4A^2/aN_0$.)

Equation (64) is the minimum value for σ_Φ^2 due to the effects of fluctuations of both the process θ and the noise $N_c(t,\Phi)$. The bandwidth a_0 of equation (64) is smaller than B_2 of equation (45) because of the *a priori* statistics of the process θ which were designed into the filter F(s).

Determining of Off-Axis Tilt by Optical Feedback

Suppose that a plane wave is incident on the entrance aperture of a shearing interferometer. Assume that the incident phasefront has some x-tilt as shown in Figure 11. It will be shown that by varying the speed of the rotating grating using a feedback network, the off axis tilt in the x-direction can be determined. That is, optical rather than electrical feedback is used.

The optical field can be written as (Ref. 18, pg 49)

$$E(x,y) = E_0 \exp[jk\cos\theta x] \tag{69}$$

From the earlier analysis of the shearing interferometer the linear velocity of the grating was $v = rw_0$ (a constant speed) and the grating transmittance function $g(x_1-vt)$ was stated by equation (3). If the linear velocity is allowed to vary, then the grating transmittance function becomes $g(x_1-r\int_o^t w_1(\alpha)d\alpha)$ where vt has been replaced by $r\int_o^t w(\alpha)d\alpha$. The spatial Fourier transform of this new grating function becomes

$$\left.\begin{aligned} \mathcal{F}[g(x_1-r\textstyle\int_o^t w_1(\alpha)d\alpha)] \quad &\propto \quad G(x_2-r\textstyle\int_0^t w_1(\alpha)d\alpha) \\ f_x &= \frac{x_2}{\lambda f} \\ f_y &= \frac{y_2}{\lambda f} \end{aligned}\right|$$

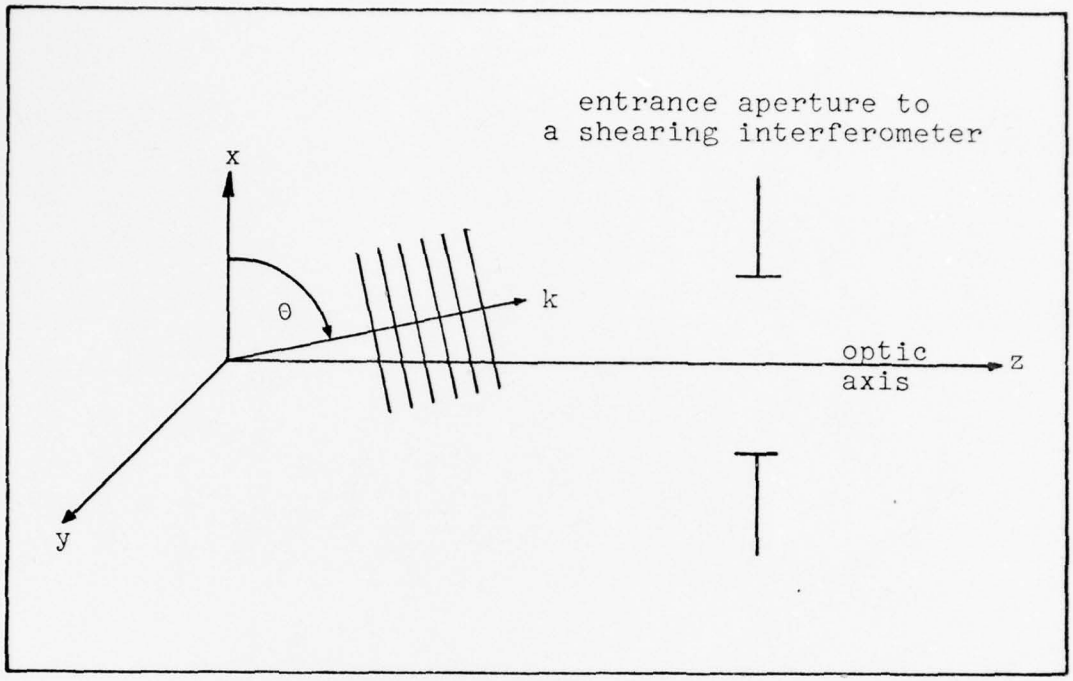

Figure 11. Plane wave with x-tilt incident on a shearing interferometer

$$= \sum_n \exp[-j\frac{kx_2}{f}(r\int_0^t w_1(\alpha)d\alpha)]A_n\delta(x_2-\frac{n\lambda f}{d})\delta(f_y) \qquad (70)$$

The electric field at the detector plane becomes (from equation (8))

$$U_d(x_2,y_2) = w(-x_2,-y_2) \circledast G(x_2-r\int_0^t w_1(\alpha)d\alpha)$$

$$= \int_{-\infty}^{+\infty} E_0\exp[jk\cos\theta(x-x')]\exp[-j\frac{kx'}{f}r\int_0^t w_1(\alpha)d\alpha]$$

$$\cdot \sum_n A_n\delta(x'-\frac{n\lambda f}{d})dx'\delta(f_y)$$

$$+ E_0 \exp[jk\cos\theta x] \int_{-\infty}^{+\infty} \exp[-j\frac{kx'}{f}(r\int_0^t w_1(\alpha)d\alpha - \cos\theta)]$$

$$\cdot \sum_n A_n \delta(x' - \frac{n\lambda f}{d})dx' \delta(f_y)$$

$$= E_0 \exp[jk\cos\theta x] \sum_n A_n \exp[jkq\frac{n\lambda f}{d}]\delta(f_y) \qquad (71)$$

where $q = r\int_0^t w_1(\alpha)d\alpha - \cos\theta$. The intensity becomes

$$I_d = U_d U^*_d = |E_0^2|\{\sum_{m=n} A_n^2 + \sum_{m\neq n} A_n A^*_m$$

$$\cdot \exp[-jkq\frac{\lambda f}{d}(n-m)]\} \qquad (72)$$

where again n can only take on the values of 0, +1, and -1 so that double and higher order frequency terms can be neglected. This results in the following bandpass portion of equation (72)

$$I_d = |E_0|^2[(\sum_n A_n^2) + A_0 A^*_{-1} \exp[-jk(\frac{\lambda f}{d})q]$$

$$+ A_0 A^*_{+1} \exp[+jk(\frac{\lambda f}{d})q]$$

$$+ A_{-1} A^*_0 \exp[+jk(\frac{\lambda f}{d})q]$$

$$+ A_{+1} A^*_0 \exp[-jk(\frac{\lambda f}{d})q] \qquad (73)$$

where as shown in Table 1 (Chapter 2) $A_0=.5$, $A_1=(1/\pi)\exp[+j90°]$ and $A_{-1}=(1/\pi)\exp[-j90°]$. Therefore equation (73) becomes

$$I_d = |E_0|^2\{(\sum_n A_n^2) + \frac{.5}{\pi}[j\cos(kq\frac{\lambda f}{d}) + \sin(kq\frac{\lambda f}{d})$$

$$- j\cos(kq\frac{\lambda f}{d}) + \sin(kq\frac{\lambda f}{d}) - j\cos(kq\frac{\lambda f}{d})$$

$$+ \sin(kq\frac{\lambda f}{d}) + j\cos(kq\frac{\lambda f}{d}) + \sin(kq\frac{\lambda f}{d})]\}$$

$$= |E_0|^2\{(\sum_n A_n^2) + \frac{2}{\pi}\sin[\frac{2\pi}{d}r\int_0^t w_1(\alpha)d\alpha - \frac{2\pi f}{d}\cos\theta] \quad (74)$$

Let $\psi=\frac{2\pi f}{d}\cos\theta$ and $w_0t + \hat{\psi} = \frac{2\pi}{d}r\int_0^t w_1(\alpha)d\alpha$ then ignoring DC terms and amplitudes, equation (74) becomes of the form

$$I_d = \sin(w_0t + \hat{\psi}-\psi) \quad (75)$$

This signal could be used as the input to the feedback system of Figure 12 where $\hat{\psi}-\psi$ represents an error signal input to a Kalman filter as described in the last section. When $\hat{\psi} = \psi$ then no command will be sent to the grating and it will rotate at a quiescent velocity, and the off-axis tilt will be known.

Therefore by employing optical feedback to the grating and alternate technique for determining off-axis tilt is possible.

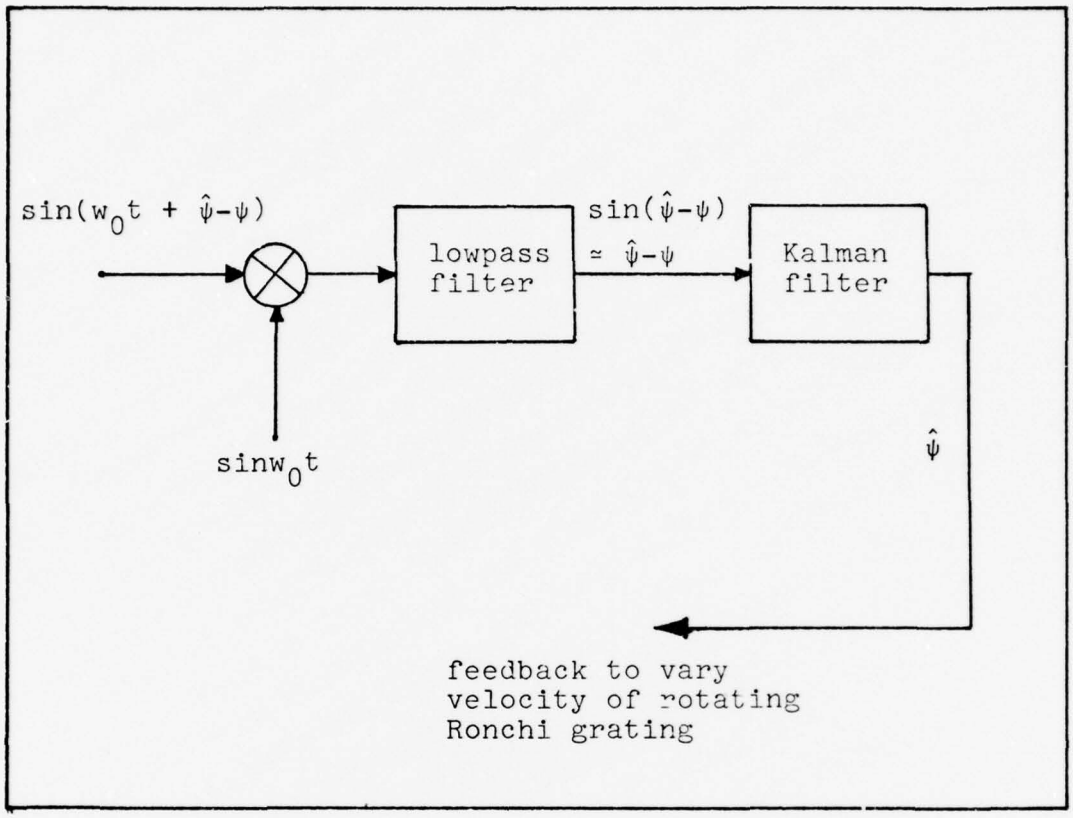

Figure 12. Optical feedback network for determining tilt

Coherent Addition of Two Detector Arrays

One of the major drawbacks to using a shearing interferometer for phasefront sensing or measurement is the poor utilization of input energy. Much of the input energy is lost due to the less than unity transmittance of the optics (which includes the lenses and Ronchi grating). In this section it is shown that the addition of another detector array appropriately located can increase the signal to noise ratio.

Assume that a detector output of a shearing interferometer is expressed as

$$s_1(t) = D\sin(w_0 t + \theta(t)) + n_1(t) \tag{76}$$

where n_1 is a zero mean random process. The signal to noise ratio for equation (76) is

$$SNR_1 = \frac{D^2}{2N_0 W} \tag{77}$$

where $D^2/2$ is the signal power, $N_0 W$ is the noise power, and W is the bandwidth.

The arrangement of Figure 13 shows a possible configuration for the addition of another detector array. The rotating Ronchi grating has been tilted at a slight angle so that the reflected portion of the field is recieved by the additional detector array. A signal at the second detector array becomes

$$s_2(t-t_d) = D\sin(w_0(t-t_d) + \theta(t-t_d)) + n_2(t) \tag{78}$$

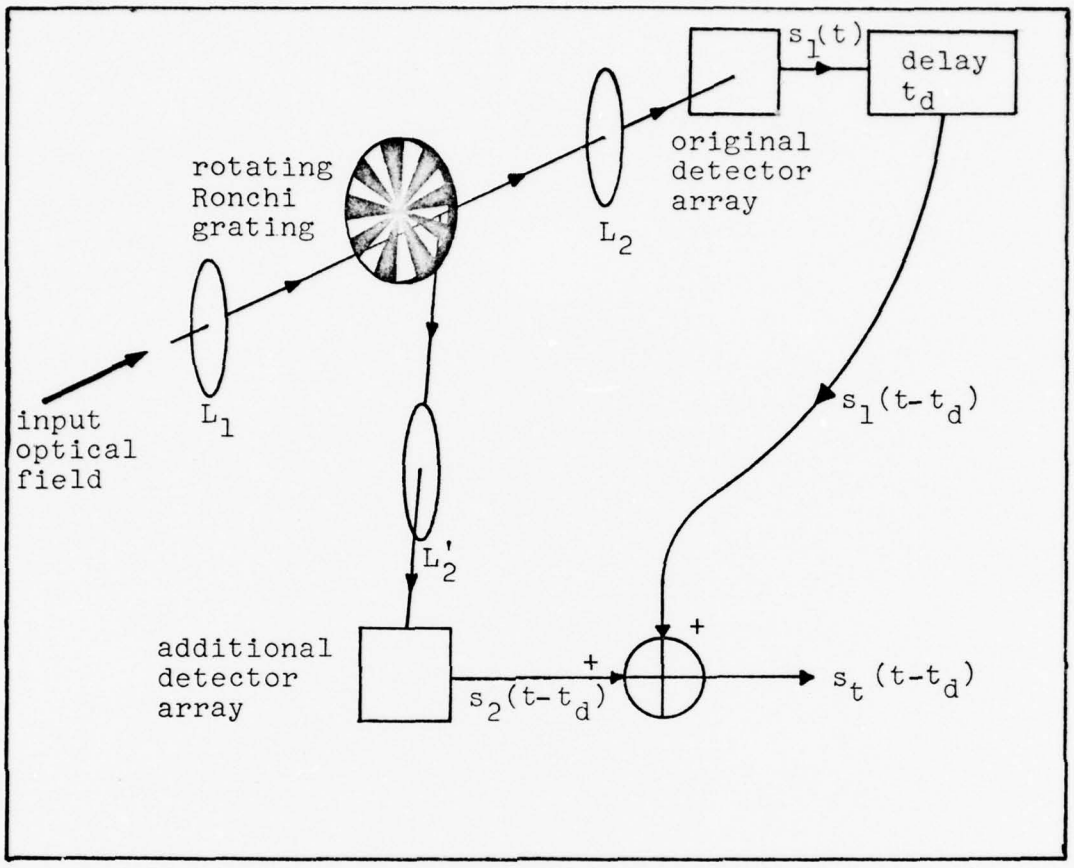

Figure 13. Arrangement for additional detector array

where t_d is the delay time with respect to the original detector array, and $n_1(t)$, $n_2(t)$ are uncorrelated and have the same power of N_0W. The delay time can be represented as

$$t_d = \frac{\text{width of spoke where image is located}}{\text{linear velocity of the grating}} \tag{79}$$

If the output of the original detector array can be delayed by t_d as shown in Figure 13, then the two signals $s_1(t)$ and $s_2(t)$ can be coherently added:

$$s_t(t-t_d) = s_1(t-t_d) + s_2(t-t_d)$$

$$= 2D\sin(w_0(t-t_d) + \theta(t-t_d)) + n_1(t) + n_2(t) \quad (80)$$

For equation (80) the signal power is $2D^2$ and the noise power becomes $E[(n_1(t) + n_2(t))^2] = 2N_0W$. The signal to noise ratio now becomes

$$SNR_2 = \frac{D^2}{N_0W} \quad (81)$$

which is an improvement of 3dB over the result of equation (77). This result assumes that the entire input field is reflected into the second detector array rather than scattered.

IV Representation of a Distorted Phasefront

A geometric representation of a distorted phasefront will be provided in this chapter (Refs. 19, pg 1427-1435; 20, pg 144-154; 21, pg 464-466). This representation can be made up of parameters such as tilt, defocus, and astigmatism which are understood optics terms.

Fried (Ref. 19) derives a description of the phasefront shape by fitting the distorted phase profile with a polynomial. It is assumed that the distorted phase profile is received by a circular aperture of diameter d. A set of orthonormal polynomials which are closely related to Zernike polynomials (Ref. 21) are used. The six orthonormal polynomials are defined as follows (where R = d/2 and ρ defines the polar representation of x and y coordinates in the receiving aperture):

$$Z_1(\rho) = (1/\pi R^2)^{1/2} \tag{82}$$

which is used to represent an overall phase shift,

$$Z_2(\rho) = (4/\pi R^4)^{1/2} x \tag{83}$$

and

$$Z_3(\rho) = (4/\pi R^4)^{1/2} y \tag{84}$$

are used to represent x and y tilt respectively. The focus term is represented by

$$Z_4(\rho) = (12/\pi R^6)^{1/2}(x^2 + y^2 - R^2/2) \tag{85}$$

and astigmatism is represented by

$$Z_5(\rho) = (6/\pi R^6)^{1/2}(x^2 + y^2) \tag{86}$$

and

$$Z_6(\rho) = (24/\pi R^6)^{1/2} xy \tag{87}$$

The distorted phase can be approximated by

$$\phi(\rho) = \sum_{j=1}^{6} a_j Z_j(\rho) \tag{88}$$

where the expansion coefficients a_j are defined by

$$a_j = \int_{-\infty}^{+\infty} d\rho \xi(\eta;d)\phi(\rho)Z_j(\rho) \tag{89}$$

where $\eta = |\rho|$, $\xi(\eta;d)$ is the receiving aperture function

$$\xi(\eta;d) = \begin{cases} 1 & \text{if } |\rho|<R \\ 0 & \text{if } |\rho|>R \end{cases} \tag{90}$$

and

$a_1 \propto$ degree of phase shift of the phasefront

$a_2 \propto$ extent of random x-tilt

$a_3 \propto$ extent of random y-tilt

$a_4 \propto$ extent of defocus

$a_5 + a_6 \propto$ extent of astigmatic deformation

As mentioned earlier, the measurements made by the shearing interferometer consist of twelve phase difference measurements $\theta \propto \phi(x_2-s) - \phi(x_2+s)$. The basic definition of a derivative implies that

$$\theta \simeq \frac{\partial \phi}{\partial x} \quad (\text{or } \frac{\partial \phi}{\partial y} \text{ for y-shear}) \tag{91}$$

when the shear distance is small. Equation (88) now becomes (for x-shear)

$$\theta \simeq \frac{\partial \phi(x,y)}{\partial x} = \sum_{j=1}^{6} a_j \frac{\partial Z_j(x,y)}{\partial x} \tag{92}$$

In matrix form, equation (92) becomes

$$\underline{\theta} = [\frac{\partial}{\partial x}(\underline{Z})]\underline{a} \tag{93}$$

where $\underline{\theta}$ is a (12×1) vector of phase difference measurements provided by the phasefront sensor (six from the x-channel interferometer and six from the y-channel interferometer). The quantity $[\frac{\partial}{\partial x}(\underline{Z})]$ is a (12×6) matrix of twelve rows of appropriate partial derivatives of equations (82) to (87), and $\underline{a}$ is a (6×1) vector containing $(a_1\text{-}a_6)$. Equation (93) has twelve equations and six unknowns $(a_1\text{-}a_6)$. This overdetermined system can be solved by the method of least squares. (See Ref. 22 for a contrasting approach.) Since $[\frac{\partial}{\partial x}(\underline{Z})]$ is rectangular, it does not posess an inverse; therefore, in order to find $\underline{a}$ the technique of generalized inverses must be used. (A similar procedure for generalized inverses is found in Refs. 23 and 24.) Equation (93) can be rewritten as

$$\underline{a} = [\frac{\partial}{\partial x}(\underline{Z})]^{+}\underline{\theta} \tag{94}$$

where

$$[\frac{\partial}{\partial x}(\underline{Z})]^{+} \triangleq [[\frac{\partial}{\partial x}(\underline{Z})]^{T}[\frac{\partial}{\partial x}(\underline{Z})]]^{-1}[\frac{\partial}{\partial x}(\underline{Z})]^{T} \tag{95}$$

which is the generalized inverse of $[\frac{\partial}{\partial x}(\underline{Z})]$, and $\underline{a}$ is a best approximate solution of a_1 through a_6.

In practice $\underline{\theta}$ is a (12×1) vector of $\hat{\theta}$'s which are obtained from the phaselocked loop of the previous chapter. Therefore, $\underline{\hat{a}}$ is actually found from equation (94). The relationship between $\sigma^2_{\underline{\hat{\theta}}}$ and $\sigma^2_{\underline{\hat{a}}}$ is derived as follows

$$\text{cov}[\underline{\hat{a}}] = E[(\underline{\hat{a}} - E[\underline{\hat{a}}])(\underline{\hat{a}} - E[\underline{\hat{a}}])^{T}] \tag{96}$$

$$= [\frac{\partial}{\partial x}(\underline{Z})]^{+}E[(\underline{\hat{\theta}} - E[\underline{\hat{\theta}}](\underline{\hat{\theta}} - E[\underline{\hat{\theta}}])^{T}][\frac{\partial}{\partial x}(\underline{Z})]^{+^{T}} \tag{97}$$

$$= [\frac{\partial}{\partial x}(\underline{Z})]^{+}\text{cov}[\underline{\hat{\theta}}][\frac{\partial}{\partial x}(\underline{Z})]^{+^{T}} \tag{98}$$

Based on earlier results the diagonal terms can be found. The cross terms of $\text{cov}[\underline{\hat{\theta}}]$ are nonzero since the $\hat{\theta}$'s are correlated. These cross terms cannot be easily found.

In summary, the output of the phasefront sensor consists of twelve phase difference measurements which can be used to find $\underline{\hat{a}}$ in a computer implementation. Then the obtained values of a_1 through a_6 can be translated into control commands to correct for random tilting of the phasefront, defocus, and astigmatism introduced by the turbulent atmosphere.

V Conclusion

Summary

This paper first presented a description of operation for a shearing interferometer. It was shown that the interferometer's output were signals with phases which were a function of a phasefront's spatial phase.

The output signal processing was studied using a basic demodulation scheme and then compared to a design using phase-locked loops and some optimal linear filtering theory. Some basic phaselocked loop theory was provided.

A possible configuration using optical feedback for determining off-axis tilt of a plane was discussed. It was found that by varying the speed of the rotating grating, the off-axis tilt of an incident planar phasefront could be determined.

An improvement in signal-to-noise ratio was achieved by a slight modification of the shearing interferometer. This modification consisted of adding an additional detector array to collect energy reflected off of the rotating grating and coherently adding the signals of both detector arrays.

Finally, a geometric representation of a distorted phase-front was provided. It was shown that the distorted phasefront could be represented by terms such as tilt, defocus, and astigmatism.

Suggestions for Further Study

In this paper, noise contributed by dark current and thermal effects was ignored. These effects on the performance of several signal processing schemes should be studied.

The fact that the phase of each signal is spatially correlated could be used to design a better signal processing arrangement.

Finally, the study of alternate systems for phasefront sensing could be contrasted to the operation of the shearing interferometer.

The problem of least square fitting a phasefront estimate to find an array of phase difference measurements is discussed in Ref. 25, pg 370.

Bibliography

1. Fried, D. L., "Propagation of a Spherical Wave in a Turbulent Medium," J. Opt. Soc. Amer., Vol 57, No. 2, pg 175-180, 1967.

2. Strohbehn, J. W., "Line-of-Sight Propagation Through the Turbulent Atmosphere," Proceedings of the IEEE, Vol 56, pg 1301-1318, 1968.

3. Tatarski, V. I., Wave Propagation in a Turbulent Medium, McGraw-Hill Book Company, New York, 1961.

4. Gagliardi, R. M., and Karp, S., Optical Communications, John Wiley & Sons, New York, 1976, pg 13.

5. Fried, D. L., and Yura, H. T., "Telescope-Performance Reciprocity for Propagation in a Turbulent Medium," J. Opt. Soc. Amer., Vol 62, pg 600, 1972.

6. Hardy, J. W., "Active Optics: A New Technology for the Control of Light," Proceedings of the IEEE, June 1977.

7. Wyant, J. C., "Double Frequency Grating Lateral Shear Interferometer," Applied Optics, Vol 12, No. 9, 1973.

8. Wyant, J. C., "Use of an ac heterodyne lateral shear interferometer with real time wavefront correction systems," Applied Optics, Vol 14, No. 11, 1975.

9. Hardy, J. W., et al., "Real-time atmospheric compensation," J. Opt. Soc. Amer., Vol 67, No. 3, 1977.

10. Françon, M., Optical Interferometry, Academic Press, New York, 1966.

11. Spiegel, M., Schaums Outline on Fourier Analysis, McGraw-Hill, New York, 1974.

12. Viterbi, A. J., Principles of Coherent Communication, McGraw-Hill, New York, 1966.

13. Lindsey, W. C., Synchronization Systems in Communications and Control, Prentice-Hall, New Jersey, 1972.

14. Ziemer, R. E., and Tranter, W. H., Principles of Communications, Houghton Miffin Company, Boston, 1976.

15. Taub H., and Shilling D., Principles of Communication Systems, McGraw-Hill, New York, 1971.

16. Van Trees, H. L., Detection, Estimation, and Modulation Theory, John Wiley and Sons, New York, 1968.

17. Gelb, A., Applied Optimal Estimation, M.I.T. Press, Cambridge, Massachusetts, 1974.

18. Goodman, J., Introduction to Fourier Optics, McGraw-Hill, San Francisco, 1968.

19. Fried, D. L., "Statistics of a Geometric Representation of Wavefront Distortion," J. Opt. Soc. Amer., Vol 55, No. 11, 1965.

20. Hogge, C. B., and Butts, R. R., "Frequency Spectra for the Geometric Representation of Wavefront Distortions Due to Atmospheric Turbulence," IEEE Transactions of Antennas and Propagation, Vol AP-24, No. 2, 1976.

21. Born, M., Wolf, E., Principles of Optics, Pergamon Press, New York, 1975.

22. Rimmer, M. P., "Method for Evaluating Lateral Shearing Interferograms," Applied Optics, Vol. 13, No. 3.

23. Noble, B., and Daniel, J., Applied Linear Algebra, second edition, Prentice-Hall, N. J., 1977.

24. Rao, C., and Mitra S., Generalized Inverse of Matrices and its Applications, John Wiley and Sons, New York, 1971.

25. Fried, D. L., "Least Square Fitting A Wavefront Distortion Estimate to an Array of Phase-Difference Measurements," J. Opt. Soc. Amer., Vol 67, No. 3, 1977.

Appendix

Intensity at the Shearing Interferometer Detector Plane assuming Sheared Amplitudes are not Equal

As stated in Chapter 2, the detector plane intensity can be expressed as

$$\begin{aligned} I_d(x_2,y_2) &= U_d(x_2,y_2)U_d^*(x_2,y_2) \\ &= [V_0 + V_{+1} + V_{-1}][V_0 + V_{+1} + V_{-1}]^* \\ &= V_0V_0^* + V_{+1}V_{+1}^* + V_{-1}V_{-1}^* + V_{+1}V_0^* + V_{+1}V_{-1}^* \\ &\quad + V_{-1}V_0^* + V_{-1}V_{+1}^* + V_0V_{+1}^* + V_0V_{-1}^* \end{aligned} \qquad (A\text{-}1)$$

where * denotes the complex conjugate of the designated quantity. The detector electronics filters out the DC terms ($V_0V_0^*$, $V_{+1}V_{+1}^*$, and $V_{-1}V_{-1}^*$) and the time varying terms of $2w_0$ ($V_{+1}V_{-1}^*$ and $V_{-1}V_{+1}^*$). Therefore the information bearing portion of equation (A-1) becomes

$$\begin{aligned} I_d(x_2,y_2) &\simeq [V_{+1}V_0^* + V_0V_{+1}^*] + [V_{-1}V_0^* + V_0V_{-1}^*] \\ &= 2\text{Real}\{V_0V_{+1}^*\} + 2\text{Real}\{V_{-1}V_0^*\} \\ &= 2A_0A_{+1}^*A_{inc}(x_2,y_2)A_{inc}(x_2+s,y_2) \\ &\quad \cdot \cos[w_0t - \phi(x_2+s,y_2) + \phi(x_2,y_2)] \\ &\quad + 2A_{-1}A_0^*A_{inc}(x_2,y_2)A_{inc}(x_2-s,y_2) \\ &\quad \cdot \cos[w_0t + \phi(x_2-s,y_2) - \phi(x_2,y_2)] \end{aligned} \qquad (A\text{-}2)$$

where V_0 , V_{+1} , and V_{-1} are defined in equation (10). Neglecting common factors equation (A-2) becomes

$$I_d \propto A_{inc}(x_2+s,y_2)\cos[w_0t - \phi(x_2+s,y_2) + \phi(x_2,y_2)] + A_{inc}(x_2-s,y_2)\cos[w_0t + \phi(x_2-s,y_2) - \phi(x_2,y_2)] \tag{A-3}$$

which is of the form

$$A'\cos[w_0t + \phi'] + A''\cos[w_0t + \phi''] \tag{A-4}$$

Using phasor notation with an implied radian frequency of w_0 equation (A-4) becomes

$$[(A'_x + A''_x)^2 + (A'_y + A''_y)^2]^{1/2}\exp[j\tan^{-1}(\frac{A'_y + A''_y}{A'_x + A''_x})] \tag{A-5}$$

where $A'_x = A'\cos\phi'$, $A'_y = A'\sin\phi'$, $A''_x = A''\cos\phi''$, and $A''_y = A''\sin\phi''$. Including the frequency dependence of the phasor expression, equation (A-5) can be written as

$$[(A'_x + A''_x)^2 + (A'_y + A''_y)^2]^{1/2}\cos[w_0t + \tan^{-1}(\frac{A'_y + A''_y}{A'_x + A''_x})] \tag{A-6}$$

Equation (A-6) is a general result for the information bearing portion of the intensity at the detector plane.

For the case discussed in Chapter 2 where it is assumed that $A_{inc}(x_2,y_2) \approx A_{inc}(x_2+s,y_2) \approx A_{inc}(x_2-s,y_2)$ then

$$\tan^{-1}\left(\frac{A'_y + A''_y}{A'_x + A''_x}\right) = \tan^{-1}\left(\frac{\sin(1/2(\phi'+\phi''))\cos(1/2(\phi'-\phi''))}{\cos(1/2(\phi'+\phi''))\cos(1/2(\phi'-\phi''))}\right)$$

$$= 1/2(\phi'+\phi'')$$

$$= \frac{\phi(x_2-s,y_2) - \phi(x_2+s,y_2)}{2} \qquad \text{(A-7)}$$

Therefore equation (A-6) becomes proportional to equation (14) when the sheared amplitudes are approximately equal.

Vita

Patrick J. Martone was born on 26 October 1955 in Geneva, New York. He graduated from Arlington High School, Arlington, Massachusetts, in 1973. He attended the University of Lowell, (formerly Lowell Technological Institute) Lowell, Massachusetts from 1973-1977 where he graduated cum laude with a Bachelor of Science degree in Electrical Engineering. Upon graduation, he received a commission as a second lieutenant in the U.S. Air Force and entered active duty on 2 June 1977 as a resident graduate student at the School of Engineering, Air Force Institute of Technology.

Permanent address: 48 Brantwood Road
Arlington, Massachusetts 02174

Unclassified

SECURITY CLASSIFICATION OF THIS PAGE (When Data Entered)

REPORT DOCUMENTATION PAGE		READ INSTRUCTIONS BEFORE COMPLETING FORM
1. REPORT NUMBER AFIT/GEO/EE/78-2	2. GOVT ACCESSION NO.	3. RECIPIENT'S CATALOG NUMBER
4. TITLE (and Subtitle) SIGNAL PROCESSING FOR SHEARING INTERFEROMETER MEASUREMENTS		5. TYPE OF REPORT & PERIOD COVERED MS Thesis 6. PERFORMING ORG. REPORT NUMBER
7. AUTHOR(s) Patrick J. Martone 2nd Lt USAF		8. CONTRACT OR GRANT NUMBER(s)
9. PERFORMING ORGANIZATION NAME AND ADDRESS Air Force Institute of Technology (ATC) AFIT/EN Wright-Patterson AFB, OH 45433		10. PROGRAM ELEMENT, PROJECT, TASK AREA & WORK UNIT NUMBERS
11. CONTROLLING OFFICE NAME AND ADDRESS		12. REPORT DATE December 1978 13. NUMBER OF PAGES 59
14. MONITORING AGENCY NAME & ADDRESS(if different from Controlling Office) Air Force Weapons Laboratory (AFWL/ALO) Air Force Systems Command Kirtland AFB, NM		15. SECURITY CLASS. (of this report) 15a. DECLASSIFICATION/DOWNGRADING SCHEDULE

16. DISTRIBUTION STATEMENT (of this Report)

Approved for public release; distribution unlimited

17. DISTRIBUTION STATEMENT (of the abstract entered in Block 20, if different from Report)

18. SUPPLEMENTARY NOTES

Approved for public release; IAW AFR 190-17

JOSEPH P. HIPPS, Major, USAF
Director of Information 1-23-79

19. KEY WORDS (Continue on reverse side if necessary and identify by block number)

Shearing Interferometer
Signal Processing of Spatial Phase Measurements
Optical Phase Processing

20. ABSTRACT (Continue on reverse side if necessary and identify by block number)

This paper provides a basic description of the operation of a shearing interferometer used for phasefront sensing. The signal processing of the interferometer's outputs are studied. A basic demodulation scheme and a phaselocked loop configuration are discussed and compared. Some elementary phaselocked loop theory is provided. A possible configuration using optical feedback for determining off-axis tilt of a plane is presented. The signal-to-noise ratio of the shearing interferometer's outputs is

DD FORM 1 JAN 73 1473 EDITION OF 1 NOV 65 IS OBSOLETE

Unclassified

SECURITY CLASSIFICATION OF THIS PAGE (When Data Entered)

improved by a slight modification of the optical configuration. Finally, a geometric representation of a distorted phase profile is provided which will describe the deleterious effects of a planar phasefront propagating through the turbulent atmosphere.